A Simple Method for Passivity Enhancement of Current Controlled Grid-Connected Inverters

Akhavan, Ali; Vasquez, Juan C.; Guerrero, Josep M.

Published in:
IEEE Transactions on Power Electronics

DOI (link to publication from Publisher):
10.1109/TPEL.2020.2967239

Publication date:
2020

Document Version
Accepted author manuscript, peer reviewed version

A Simple Method for Passivity Enhancement of Current Controlled Grid-Connected Inverters

Ali Akhavan, *Member, IEEE,* Juan C. Vasquez, *Senior Member, IEEE,* and Josep M. Guerrero, *Fellow, IEEE*

***Abstract*- Grid-connected inverters with *LCL* filter work stable using active damping methods. However, the stability of the control system can be threatened easily by grid impedance variation. On the other hand, delay in digitally-controlled systems shrinks the stable region. Therefore, it is very probable that by variation of grid impedance, resonance frequency located in the unstable region. To address this problem, a simple but effective method based on converter-side current feedback is proposed in this paper. This method does not need any extra sensors for active damping, which increases reliability and reduces the cost. The proposed method expands the stable region and guarantees the stability of the inverter against the grid impedance variation. It is shown that the proposed method is effective in the case of multi-paralleled inverters whiles normally coupling effect among inverters makes the stability condition worse. The effectiveness of the proposed method is verified through experimental results.**

***Index Terms*—Active damping, delay, grid-connected inverter, multi-paralleled inverters, passivity, stability**

I. Introduction

The resonance of the *LCL* filter may interact with the control loops, resulting in harmonic instability [1]. Various damping methods, i.e., passive and active damping methods have been well documented in [2]. It has been found that delay in digitally-controlled systems has a destabilizing effect within the single-loop control system. Given the time delay of $1.5T_s$, where $T_s = 1/f_s$ is the sampling period, it was found that the converter-side current control can be designed stable for the *LCL* resonance frequency below $f_s/6$ without any damping methods [3]. However, the variation of grid impedance could locate the resonance frequency outside of the stable region, which causes instability.

Continuous research efforts have been made to mitigate the delay effect in the control system. A first-order high-pass filter is used in [4] for delay compensation, which is prone to noise amplification. Also, It is not sufficient if the resonance frequency is higher than $f_s/3$. The reciprocal of a notch filter is used in [5] for compensation of the phase lag caused by the delay. To reduce the delay, a method is shifting the sampling instant of the capacitor current, proposed in [6], which is susceptible to signal aliasing and switching noise. In [7], a repetitive block is proposed for delay compensation, which expands the stable region at the cost of infinite gain and noise amplification at the Nyquist frequency ($f_s/2$).

The other challenge associated with renewable-based plants is the coupling effect among inverters [8]–[10]. In a microgrid with multi-paralleled inverters, all of the inverters are coupled through the grid impedance Z_g. Hence, despite the variation of grid impedance, connection or disconnection of an inverter changes the impedance seen by other inverters and should be considered in controller design to prevent instability.

In this paper, a delay compensation method based on biquad filter is proposed, which guarantees the stability of grid-connected inverters against the grid impedance variation and coupling effect among paralleled inverters. The proposed method only uses converter-side current in the control system and it does not need any other active damping methods. Therefore, it reduces the cost and increases the reliability.

The main contribution of this paper is stabilizing *LCL*-filtered grid-connected inverters in weak grids without any extra sensors. This method increases the critical frequency by using the biquad filter and hence, expands the inverter's stable operation region. Many delay compensation methods are based on introducing a positive phase to the system, which normally comes from lead-lag controllers to amend the phase lag caused by the delay. However, the superiority of the biquad filter in comparison with other types of band-pass filters can be expressed by the value of the positive phase, which introduces to the system. Almost all common band-pass filters normally introduce a positive phase up to 90°, while by using the biquad filter, it is possible to introduce a higher positive phase. In addition, since the inverter output admittance remains passive over a wide range of frequency, the stability of the system in the case of multi-paralleled inverters is guaranteed whiles normally coupling effect among inverters makes the stability condition worse [8], [9]. Also, the proposed method does not need any adaptive algorithms based on online grid impedance estimation to tune the control parameters and resonance damping, such as used in [11], [12].

The rest of this paper is organized as follows. In Section II, the non-stable region of the control system is presented to formulate the problem. The passivity enhancement method is proposed in Section III. In Section IV, the proposed method is validated through experimental results on a lab prototype considering grid impedance variation and coupling effect among inverters. Finally, Section V, concludes the paper.

Manuscript received October 27, 2019; revised December 2, 2019 and December 25, 2019; accepted January 13, 2020. *(Corresponding author: Ali* Akhavan.*)*

The authors are with the Department of Energy Technology, Aalborg University, Aalborg 9220, Denmark (e-mail: alak@et.aau.dk; juq@et.aau.dk; joz@et.aau.dk).

This work was funded by a Villum Investigator grant (no. 25920) from The Villum Fonden.

This article has been accepted for publication in a future issue of this journal, but has not been fully edited. Content may change prior to final publication. Citation information: DOI 10.1109/TPEL.2020.2967239, IEEE Transactions on Power Electronics

II. System Description and Problem Definition

Fig. 1 shows the circuit of a three-phase *LCL*-filtered grid-connected inverter with the single-loop current control, where Z_{L1}, Z_{L2}, Z_C and Z_{Lg} are the inverter-side inductor impedance, the grid-side inductor impedance, the capacitor impedance and the grid impedance, respectively.

$$Z_{L1} = L_1 s,\ Z_{L2} = L_2 s,\ Z_C = \frac{1}{Cs},\ Z_{Lg} = L_g s \tag{1}$$

Also, Fig. 2 shows the per-phase single-loop control block diagram of the grid-connected inverter. In this figure, $G_i(s)$ is the proportional-resonant current controller and $G_d(s)$ models the computational and the PWM delay ($G_d(s) = e^{-1.5T_s s}$). The amplitude of triangular carrier signal is considered $V_{tri} = V_{dc}/2$. Therefore, the transfer function from the modulation signal to the inverter bridge voltage is equal to 1 and its block is not shown in Fig. 2.

To show the non-stable region of the single-loop control system, the impedance model can be derived using Fig. 2.

$$i_1(s) = G_{cl}(s) i_{ref}(s) - Y_o(s) V_c(s) \tag{2}$$

where, $G_{cl}(s)$ is the closed-loop transfer function and $Y_o(s)$ is the inverter output admittance which is given by

$$Y_o(s) = \left.\frac{i_1(s)}{V_c(s)}\right|_{i_{ref}=0} = \frac{1}{sL_1 + G_i(s)G_d(s)} \tag{3}$$

The Norton equivalent circuit of a grid-connected inverter is shown in Fig. 3. As shown in this figure, the capacitor C and the grid-side inductor L_2 could be regarded as a part of grid impedance. As stated in passivity-based theory, a grid-connected inverter will be stable if it satisfies the following constraints: 1) the closed-loop transfer function of the control system should not have RHP poles and 2) the phase of $Y_o(s)$ should be within [−90°, 90°] [13]–[16]. Regarding this constraint, the system will be stable regardless of the grid impedance and the number of paralleled inverters.

The resonant part of PR controller can be neglected at

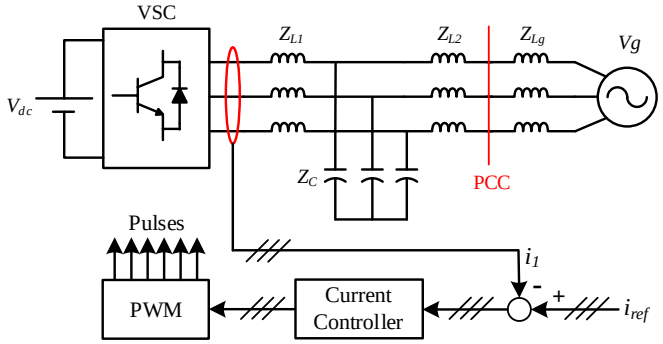

Fig. 1. Three-phase *LCL*-filtered inverter with the single-loop control.

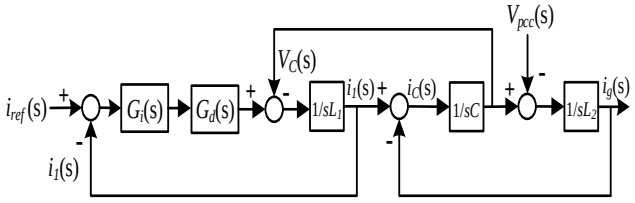

Fig. 2. Per-phase block diagram of a three-phase *LCL*-filtered inverter with the single-loop current control.

frequencies not in the vicinity of the fundamental frequency because of its negligible effect at these frequencies. Hence, the real part of $1/Y_o(s)$ could be used for predicting the passivity of the control system, since the sign of $Re\{1/Y_o(s)\}$ is equal to that of $Re\{Y_o(s)\}$. This leads to

$$Re\{\frac{1}{Y_o(j\omega)}\} = k_p \cos(1.5\omega T_s) \tag{4}$$

It is clear that $Re\{1/Y_o(s)\}$ is positive in the interval of (0, f_s/6) and it is negative in the interval of (f_s/6, f_s/2), where f_s/6 is named as critical frequency f_{cr}.

The Bode plot of $Y_o(s)$ and equivalent grid admittance $Y_{g\_eq}(s)$ are shown in Fig. 4 using the parameters listed in Table I and assuming k_p =20 (to achieve PM = 45° for loop gain). As shown in this figure, there is a wide range of frequency, which the phase of $Y_o(s)$ is beyond [−90°, 90°].

III. Passivity Enhancement

The delay causes phase lag and it limits the critical frequency to f_s/6. Therefore, to enhance the passivity, it is necessary to expand the critical frequency. In this paper, a biquad filter is proposed to compensate the phase lag and keep the inverter output admittance positive over a wide range of frequency. The proposed control system is shown in Fig. 5, where, the transfer function of the biquad filter is:

$$G_a(s) = k_a \frac{s^2 + \omega_\alpha^2}{s^2 + 2\beta\omega_\beta s + \omega_\beta^2} \tag{5}$$

The Bode plot of the biquad filter is shown in Fig. 6. The superiority of the biquad filter in comparison with other types of band-pass filters can be expressed by the value of the positive phase which introduces to the system. In other words,

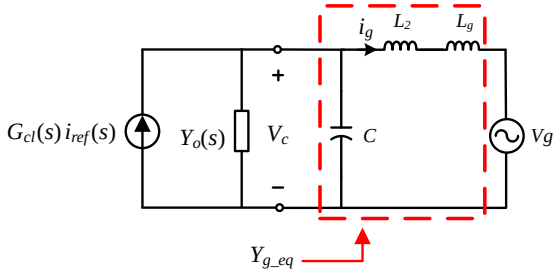

Fig. 3. Norton equivalent circuit of the converter-side current controlled grid-connected inverter.

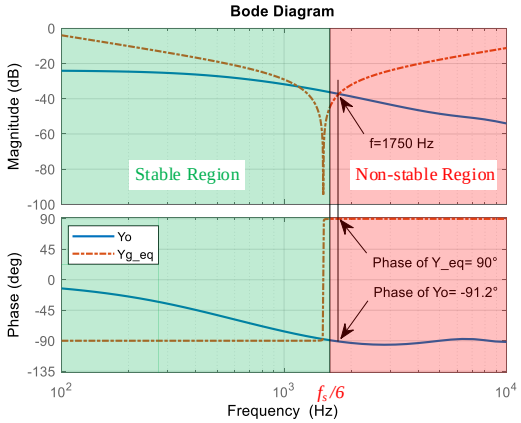

Fig. 4. The Bode plots of $Y_{o(s)}$ and Y_{g_eq} with the single-loop current control.

This article has been accepted for publication in a future issue of this journal, but has not been fully edited. Content may change prior to final publication. Citation information: DOI 10.1109/TPEL.2020.2967239, IEEE Transactions on Power Electronics

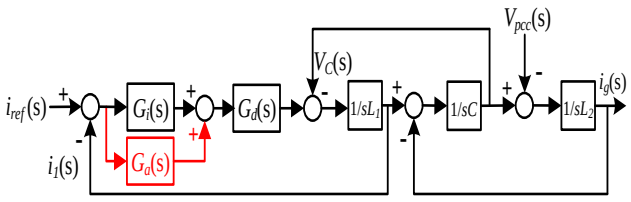

Fig. 5. Block diagram of the proposed control system.

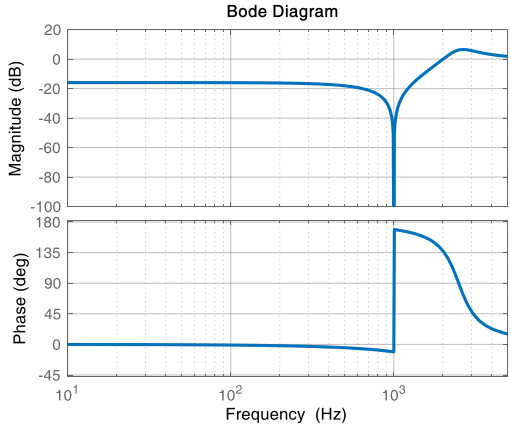

Fig. 6. The Bode plot of the biquad filter.

common band-pass filters normally introduce a positive phase up to 90°, while by using the biquad filter, it is possible to introduce a higher positive phase, as Fig. 6 shows.

To tune the parameters of the biquad filter, the inverter output admittance should be derived, at first. It can be obtained using Fig. 5, as presented in (6). The real part of $1/Y_{o\_pro}(s)$ is derived in (7) which depends on various parameters including current controller and biquad filter parameters.

$$Y_{o\_pro}(s)=\frac{1}{sL_1+(k_p+G_a(s))G_d(s)} \tag{6}$$

$$Re\{\frac{1}{Y_{o\_pro}(j\omega)}\}=[k_p+k_a\frac{(\omega_\alpha^2-\omega^2)(\omega_\beta^2-\omega^2)}{(\omega_\beta^2-\omega^2)^2+(2\beta\omega_s\omega)^2}]\cos(1.5\omega T_s)$$
$$-\frac{2\beta\omega_s\omega}{(\omega_\beta^2-\omega^2)^2+(2\beta\omega_s\omega)^2}\sin(1.5\omega T_s) \tag{7}$$

Firstly, ω_α is selected as $0.1\omega_s$ for positive phase introducing in desired frequencies which are higher than $0.1\omega_s$ (1000 Hz). In fact, selection of ω_α is based on Fig. 4, which shows the Bode plot of inverter output admittance $Y_o(s)$ for the single-loop control system. As shown in this figure, the phase

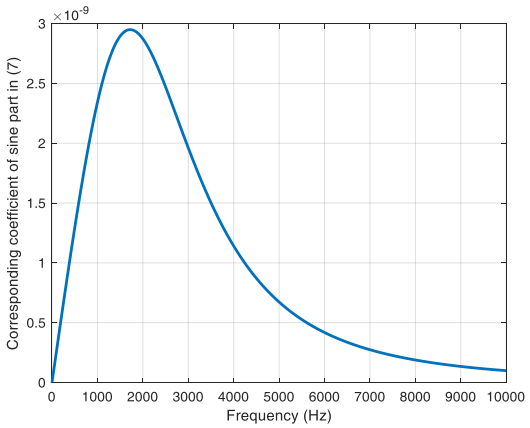

Fig. 7. The corresponding coefficient of sine part in (7) versus frequency.

of $Y_o(s)$ exceeds -90° at $f_s/6$ (1666 Hz), which means, the real part of inverter output admittance becomes negative which might cause instability. Therefore, in order to keep the real part of $Y_o(s)$ positive, it is necessary to introduce a positive phase at a frequency below $f_s/6$. Thus, ω_α is selected as $0.1\omega_s$.

Also, ω_β should be designed so that keep the magnitude of $G_a(s)$ in a reasonable range in high frequencies to prevent noise amplification. Therefore, ω_β is selected as $0.25\omega_s$. In fact, it is a fair trade-off between the magnitude of $G_a(s)$ in high frequencies and positive phase introducing.

The sign of the cosine function in (7) changes from positive to negative at $\omega=\omega_s/6$. Therefore, if the sign of multiplying part changes at this frequency, the cosine part remains positive. It leads to:

$$k_p+k_a\frac{(\omega_\alpha^2-\omega^2)(\omega_\beta^2-\omega^2)}{(\omega_\beta^2-\omega^2)^2+(2\beta\omega_s\omega)^2}\bigg|_{\omega=\omega_s/6}=0\Rightarrow$$
$$k_a=-k_p\frac{(\omega_\beta^2-\omega_s^2/36)^2+4\beta^2\omega_s^4/36}{(\omega_\alpha^2-\omega_s^2/36)(\omega_\beta^2-\omega_s^2/36)} \tag{8}$$

Using (8), k_a can be achieved as a function of k_p. In order to tune the other control parameters, i.e., k_p and β, the transfer function of the control system loop gain can be used. Using Fig. 5, the transfer function of loop gain is presented as (9).

$$T(s)=(G_i(s)+G_a(s))G_d(s)/sL_1 \tag{9}$$

The parameters k_p and β should be selected so that, $T(s)$ meet the desired cutoff frequency and desired phase margin ($PM_{\_LP\_des}$).

$$|T(j\omega)|_{\omega=\omega_{cut}}=0\,\text{dB}\Rightarrow\frac{\sqrt{\left(k_p\left[\left(-\omega^2+\omega_\beta^2\right)^2+\left(2\beta\omega_\beta\omega\right)^2\right]-k_a\left(-\omega^2+\omega_\alpha^2\right)\left(-\omega^2+\omega_\beta^2\right)\right)^2+\left(k_a\left(-\omega^2+\omega_\alpha^2\right)\left(2\beta\omega_\beta\omega\right)\right)^2}}{\left(-\omega^2+\omega_\beta^2\right)^2+\left(2\beta\omega_\beta\omega\right)^2}\times\frac{1}{\omega L_1}\bigg|_{\omega=\omega_{cut}}=1 \tag{10}$$

$$\angle T(j\omega)|_{\omega=\omega_{cut}}=PM_{PL\_des}-\pi\Rightarrow\angle\tan^{-1}\frac{k_a\left(-\omega^2+\omega_\alpha^2\right)\left(2\beta\omega_\beta\omega\right)}{k_p\left[\left(-\omega^2+\omega_\beta^2\right)^2+\left(2\beta\omega_\beta\omega\right)^2\right]-k_a\left(-\omega^2+\omega_\alpha^2\right)\left(-\omega^2+\omega_\beta^2\right)}-1.5\omega T_s\bigg|_{\omega=\omega_{cut}}=PM_{\_LP\_des}-\frac{\pi}{2} \tag{11}$$

This article has been accepted for publication in a future issue of this journal, but has not been fully edited. Content may change prior to final publication. Citation information: DOI 10.1109/TPEL.2020.2967239, IEEE Transactions on Power Electronics

TABLE I
Parameters of the inverter and grid

Parameters of inverter	
Input DC voltage, V_{dc}	650 V
Inverter-side inductor, L_1	8.6 mH
Filter capacitor, C	4.5 μF
Grid-side inductor, L_2	1.8 mH
Sampling and switching frequency	10 kHz
Rated power of each inverter	2.2 kVA
Parameters of utility grid	
Grid voltage, V_g (Phase-to-phase RMS Voltage)	400 V
Frequency	50 Hz
Grid inductance, L_g	0 mH - 3 mH

TABLE II
Control Parameters

Current controller	
k_p	15.75
k_r	800
Delay compensation controller $G_a(s)$	
k_a	149.5
β	0.205
ω_α	$0.1\omega_s$
ω_β	$0.25\omega_s$

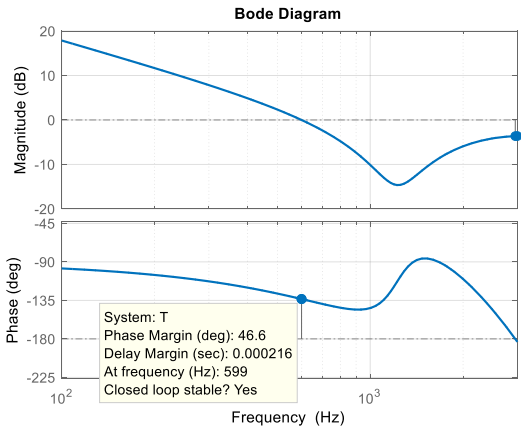

Fig. 8. Bode plot of the proposed control system loop gain.

It should be noted that, $PM_{\_LP\_des}$ is the desired phase margin associated with the loop gain of the control system ($T(s)$). By assuming $G_i(s) \approx k_p$, cutoff frequency as f_{cut} = 600 Hz ($\omega_{cut}=2\pi\times600$) and defining $PM_{\_LP\_des}$ = 45°, the equations (10) and (11) at the cutoff frequency yield which are shown at the bottom of previous page. Solving (8), (10) and (11) using numerical methods in MATLAB leads to, k_p = 15.75, k_a = 149.5 and β = 0.205. The corresponding coefficient of the sine part in (7) is depicted in Fig. 7. As shown in this figure, the magnitude of the corresponding coefficient of the sine part is very small, so it has a negligible effect on the passivity of the inverter.

The Bode plot of $T(s)$ is depicted in Fig. 8 using the control parameters listed in Table II. As shown in this figure, the cutoff frequency and $PM_{\_LP}$ are close to desirable values, i.e., 600 Hz and 45°, respectively. However, by feeding back the inverter-side current (i_1), the capacitor C and the grid-side inductor L_2 could be regarded as a part of grid impedance. In other words, the inverter is stable by considering only the inverter-side inductor as an output filter. However, its stability considering C and L_2 should be investigated using impedance-based stability criterion [17].

IV. Experimental Results

A. Stability against Grid Impedance Variation

Fig. 9 shows the inverter output admittance with single-loop current control (Y_o), the proposed method (Y_{o_pro}) and equivalent grid admittance with L_g = 1 mH ($Y_{g\_eq\_1mH}$) and L_g = 3 mH ($Y_{g\_eq\_3mH}$) with parameters presented in Table I. As

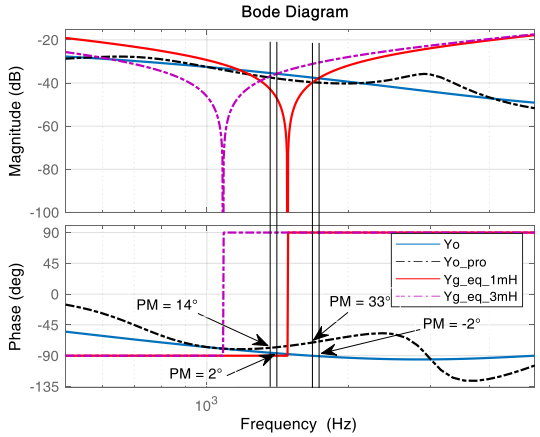

Fig. 9. The Bode plots of Y_o, Y_{o_pro}, $Y_{g\_eq\_1mH}$ and $Y_{g\_eq\_3mH}$.

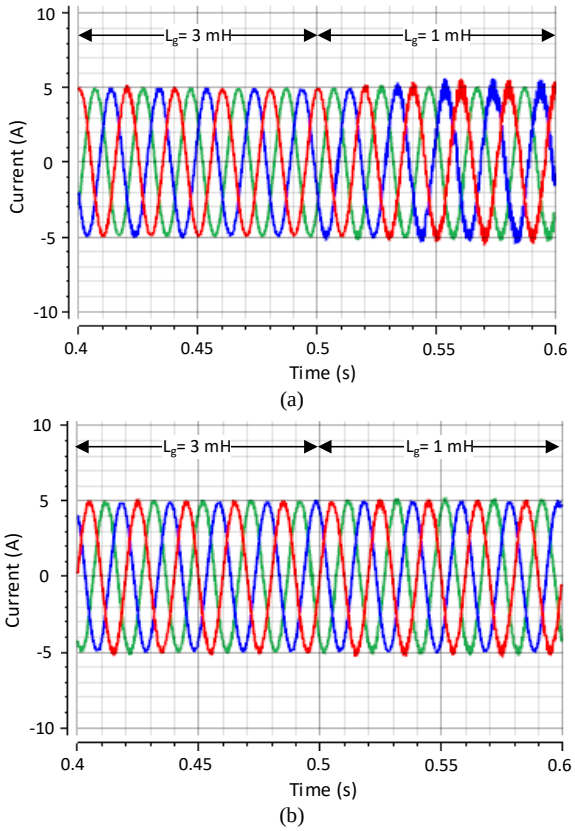

Fig. 10. The grid injected current in the grid impedance variation condition. (a) Single-loop control. (b) The proposed control system.

This article has been accepted for publication in a future issue of this journal, but has not been fully edited. Content may change prior to final publication. Citation information: DOI 10.1109/TPEL.2020.2967239, IEEE Transactions on Power Electronics

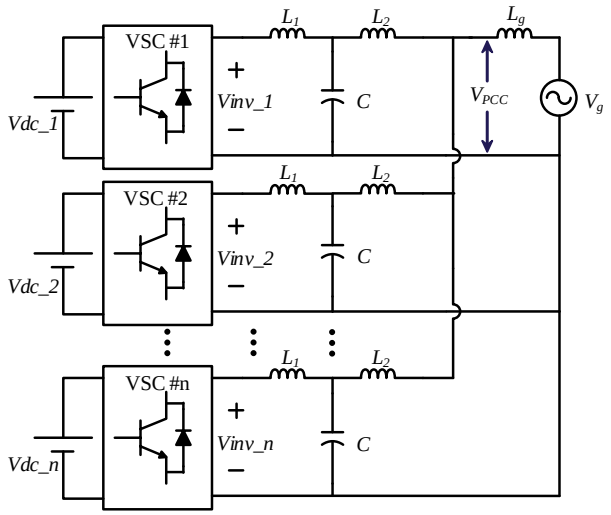

Fig. 11. Typical structure of multi-paralleled inverters in a microgrid.

shown in this figure, by using the single-loop control, when the L_g = 3 mH, the PM = 2° at the intersection point and therefore, the system is stable according to impedance-based stability criterion [10]. However, by reducing L_g to 1 mH, the PM becomes negative (PM = -2°). This shows that single-loop control is not robust against the grid impedance variation.

By using the proposed method, the PM = 14° with L_g = 3 mH and PM = 33° with L_g = 1 mH, which shows that the system is stable. It should be noted that, an increase of grid inductance, pushes the intersection point toward lower frequencies as shown in Fig. 9. Since the phase of Y_{o_pro} is higher than -90° in frequencies lower than the intersection point of Y_{o_pro} and $Y_{g\_eq\_1mH}$, it could be argued that the increase of grid inductance never makes the system unstable, which is a great achievement thanks to the proposed method.

Fig. 10(a) shows the experimental result of the grid-side current for a single-loop control system ($G_a(s)$ = 0). As shown in this figure, the grid injected current is stable with L_g = 3 mH, but it goes toward instability with the reduction of grid inductance. In the next experiment, the proposed control method is applied and the result is shown in Fig. 10(b). As shown in this figure, thanks to the proposed delay compensation method, the inverter is stable in both conditions without using any extra sensors. The experimental results verify the theoretical analysis in Fig. 9 and show the robustness of the proposed method against the grid impedance variation.

B. Multi-Paralleled Inverters

Fig. 11 shows a typical grid-connected microgrid with multi-paralleled inverters. By substituting the impedance models for the paralleled inverters (see Fig. 3), the equivalent circuit can be drawn in Fig. 12. It should be noted that, the current source for inverters are supposed to be zero (open circuit) since they have not any effects on the equivalent grid admittance seen by inverters. The equivalent grid admittance (Y_{g_eq}) for each inverter, includes the grid admittance and the inverter output admittances of the other paralleled inverters. A system consisting of two paralleled inverters is considered, for instance. Fig. 13 shows the inverter output admittance with single-loop control (Y_o) and equivalent grid admittance (Y_{g_eq}).

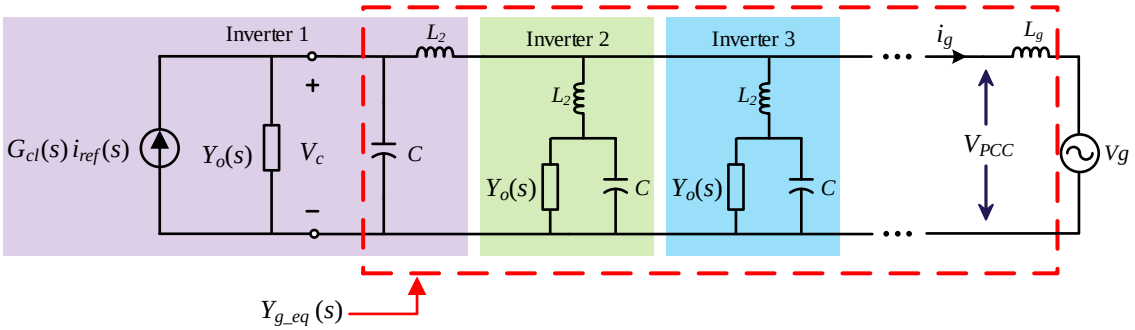

Fig. 12. Impedance-based model for multi-paralleled inverters.

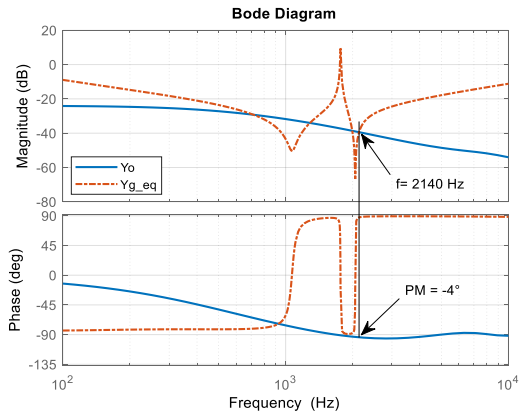

Fig. 13. The Bode plots of Y_o and Y_{g_eq} in case of connection of two inverters with the single-loop control.

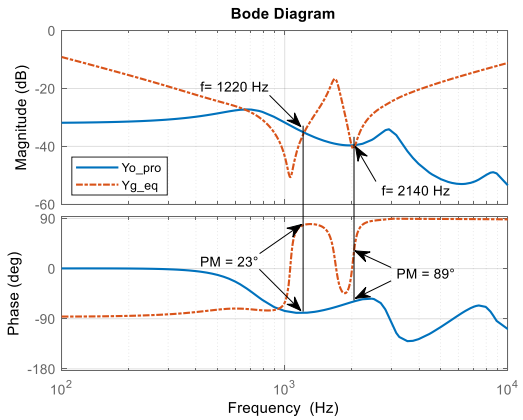

Fig. 14. The Bode plots of Y_o and Y_{g_eq} in case of connection of two inverters with the proposed control system.

This article has been accepted for publication in a future issue of this journal, but has not been fully edited. Content may change prior to final publication. Citation information: DOI 10.1109/TPEL.2020.2967239, IEEE Transactions on Power Electronics

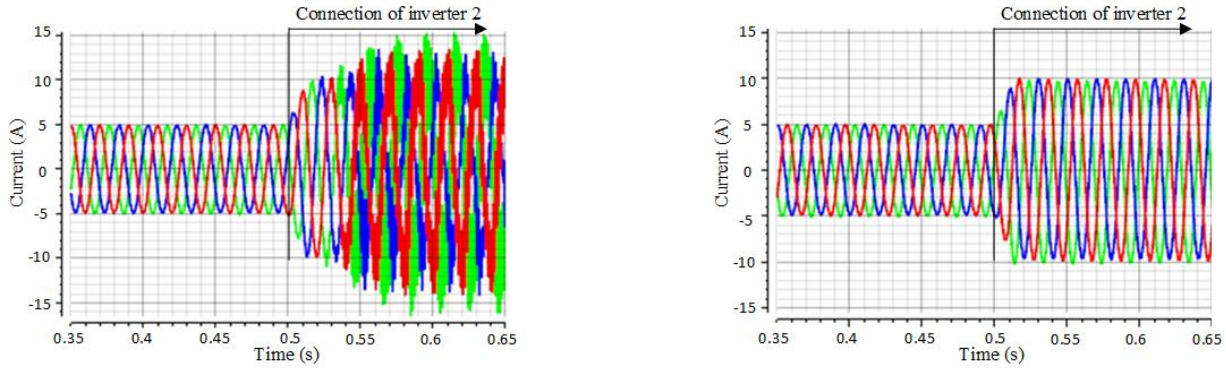

(a) (b)

Fig. 15. Total grid injected current in a system consisting of two paralleled inverters. (a) Single-loop control. (b) Proposed control system.

Both inverters are similar and L_g = 3 mH is considered. As shown in Fig. 13, the PM = -4° at the intersection point, which shows that the connection of two inverters, makes the system unstable. Fig. 14 shows the inverter output admittance using the proposed method (Y_{o_pro}) and equivalent grid admittance (Y_{g_eq}). As shown in this figure, unlike Fig. 13, the PM at the intersection points are positive which shows the effectiveness of the proposed control system in the passivity enhancement.

Fig. 15(a) shows the total grid injected current of both inverters using the single-loop control system. Inverter 1 injects its current to the grid and then, inverter 2 connects at t = 0.5 s. As shown, before connection of inverter 2, inverter 1 is stable. However, after connection of inverter 2, the system becomes unstable since equivalent grid impedance is changed. The experimental results validate the analytical results derived from Fig. 13. The experiment is repeated using the proposed control system and its result is shown in Fig. 15(b). As shown in this figure, the system remains stable after connection of inverter 2, thanks to the proposed method, which keeps the phase of the inverter output admittance within the stable region with a sufficient PM. The experimental results validate the analytical results derived from Fig. 14.

V. Conclusion

In this paper, a control system for inverters in weak grids with a wide variation of grid impedance is presented. To improve the stability, an effective method based on biquad filter is proposed, which is capable of expanding the stable region. The proposed method does not need any extra sensors for active damping which reduces the cost and increases the reliability. The control system robustness is validated in case of grid impedance wide variation and connection of parallel inverters using experimental results.

References

[1] A. Akhavan, H. R. Mohammadi, J. C. Vasquez and J. M. Guerrero, "Stability improvement of converter-side current controlled grid-connected inverters," in *Proc. 45th Annual Conference of the IEEE Industrial Electronics Society*, 2019, pp. 3943–3948.

[2] X. Ruan, X. Wang, D. Pan, D. Yang, W.i Li, and C. Bao, "Resonance damping methods of *LCL* filter," in *Control Techniques for LCL-Type Grid-Connected Inverters*, Beijing: springer, 2018.

[3] Y. Lyu, H. Lin, and Y. Cui, "Stability analysis of digitally controlled *LCL*-type grid-connected inverter considering the delay effect," *IET Power Electron.*, vol. 8, no. 9, pp. 1651-1660, Aug. 2015.

[4] X. Wang, F. Blaabjerg, and P. C. Loh, "Virtual *RC* damping of *LCL*-filtered voltage source converters with extended selective harmonic compensation," *IEEE Trans. Power Electron.*, vol. 30, no. 9, pp. 4726–4737, Sep. 2015.

[5] Z. Xin, X. Wang, P. C. Loh, and F. Blaabjerg, "Grid-current-feedback control for *LCL*-filtered grid converters with enhanced stability," *IEEE Trans. Power Electron.*, vol. 32, no. 4, pp. 3216-3228, Apr. 2017.

[6] D. Pan, X. Ruan,C.Bao,W. Li, and X.Wang, "Capacitor-current-feedback active damping with reduced computation delay for improving robustness of *LCL*-type grid-connected inverter," *IEEE Trans. Power Electron*., vol. 29, no. 7, pp. 3414–3427, Jul. 2014.

[7] X. Li, X. W. Y. Geng, X. Yuan, C. Xia, and X. Zhang, "Wide damping region for *LCL*-type grid-connected inverter with an improved capacitor current- feedback method," *IEEE Trans. Power Electron.*, vol. 30, no. 9, pp. 5247–5259, Sep. 2015.

[8] J. L. Agorreta, M. Borrega, J. López, and L. Marroyo, "Modeling and control of *N*-paralleled grid-connected inverters with *LCL* filter coupled due to grid impedance in PV plants," *IEEE Trans. Power Electron.*, vol. 26, no. 3, pp. 770-785, Mar. 2011.

[9] A. Akhavan, H. R. Mohammadi, J. C. Vasquez, and J. M. Guerrero, "Passivity-based design of plug-and-play current-controlled grid-connected inverters," *IEEE Trans. Power Electron*, vol. 35, no. 2, pp. 2135-2150, Feb. 2020.

[10] A. Akhavan, H. R. Mohammadi, and J. M. Guerrero, "Modeling and design of a multivariable control system for multi-paralleled grid-connected inverters with *LCL* filter," *Int J Electric Power Energy Syst.*, vol. 94, pp. 354–362, Jan. 2018.

[11] Y. Jing, A. A. Durra, and E. F. El-Saadany, "An adaptive digital notch filter based on grid impedance estimation for improving *LCL* filter performance," in *Proc. PES Transmission and Distribution Conference and Exposition, 2018*, pp. 1-5.

[12] N. A. Rufa'I, L. Zhang, and B. Chong, "Performance analysis of adaptive notch filter active damping methods for grid-connected converters under a varying grid impedance," in *Proc. IEEE Manchester PowerTech, 2017*, pp. 1-6.

[13] E. Rodriguez-Diaz, F. D. Freijedo, J. M. Guerrero, J. Marrero-Sosa and D. Dujic, "Input-admittance passivity compliance for grid-connected converters with an *LCL* filter," *IEEE Trans. Ind. Electron.*, vol. 66, no. 2, pp. 1089-1097, Feb. 2019.

[14] L. Harnefors, L. Zhang, and M. Bongiorno, "Frequency-domain passivity based current controller design," *IET Power Electron.*, vol. 1, no. 4, pp. 455–465, Dec. 2008.

[15] L. Harnefors, A. G. Yepes, A. Vidal, and J. Doval-Gandoy, "Passivity-based controller design of grid-connected VSCs for prevention of electrical resonance instability," *IEEE Trans. Ind. Electron.*, vol. 62, no. 2, pp. 702-710, Feb. 2015.

[16] X. Wang, F. Blaabjerg, and P. C. Loh, "Passivity-based stability analysis and damping injection for multiparalleled VSCs with *LCL* filters," *IEEE Trans. Power Electron*, vol. 32, no. 11, pp. 8922-8935, Nov. 2017.

[17] J. Sun, "Impedance-based stability criterion for grid-connected inverters," *IEEE Trans. Power Electron.*, vol. 26, no. 11, pp. 3075-3078, Nov. 2011.